www.ietdl.org

Published in IET Microwaves, Antennas & Propagation
Received on 17th January 2012
Revised on 18th April 2012
doi: 10.1049/iet-map.2012.0037



ISSN 1751-8725

Nested *U*-ring resonators: a novel multi-band metamaterial design in microwave region

O. Turkmen[1,2] *E. Ekmekci*[3] *G. Turhan-Sayan*[1]

[1]*Department of Electrical and Electronics Engineering, Middle East Technical University, Ankara, Turkey*
[2]*Department of Electronics and Telecommunications Engineering, Kocaeli University, Kocaeli, Turkey*
[3]*Department of Electronics and Communication Engineering, Suleyman Demirel University, Isparta, Turkey*
E-mail: oturkmen@metu.edu.tr

Abstract: In this study, a novel metamaterial topology, called *M*-band nested *U*-ring resonator (*M*-NURR), is proposed to provide multiple band operation with an electrically small and geometrically simple unit cell design. The *M*-NURR unit cell has *M*-nested and unconnected U-shaped metal rings printed on a dielectric substrate where each ring is primarily associated with a distinct *LC* type resonance frequency where *L* and *C* stand for inductance and capacitance, respectively. Therefore this *M*-NURR topology has the novel property that each of these resonance frequencies can be controlled almost independently by adjusting the arm length of the associated *U*-ring. In this study, three different *M*-NURR structures (for $M = 1, 2, 3$) are designed, fabricated and characterised both numerically and experimentally with very good agreement. The suggested sub-wavelength *M*-NURR metamaterial topology is anticipated to be useful in the design of miniaturised multi-band mobile communication devices as it makes the fine tuning of operation frequencies possible by a simple parametric adjustment.

1 Introduction

Metamaterials are designed, not necessarily but usually, as periodic arrays of sub-wavelength size unit cells in microwave and terahertz regions. As opposed to natural materials, they can display negative effective permittivity (ε) and/or negative effective permeability (μ) over certain frequency bands. Artificial plasma type ε-negative (ENG) metamaterials, built by periodic arrays of wires or metallic plates, have been shown to have very broad ENG bands below their plasma frequencies [1]. Arrays of conventional split ring resonator (SRR) and spiral resonator (SR) unit cells are well known topologies behaving as μ-negative (MNG) metamaterials under magnetic excitation over narrow frequency bands around their fundamental (*LC*) resonance frequencies [2]. Combining the above mentioned ENG and MNG structures within the same unit cell, metamaterials with negative refractive indices can be realised [3]. Bandwidths of resulting metamaterials are limited by the narrow-band MNG structures. In the absence of sufficiently broadband metamaterials, design of multi-band structures is highly desired for various applications in microwave and optics regimes.

It has been demonstrated that design of conventional SRR or SR unit cells with increased number of rings (or turns) helps to realise considerable amounts of miniaturisation, however, the resulting metamaterial structures still display the single-band MNG behaviour [4]. Compact multi-band MNG unit cells can be designed by using metallic inclusions having more complicated geometries as compared to the conventional SRR or SR structures [5–10]. Or alternatively, MNG topologies resonating at two or three different frequencies can be designed by using periodic arrays of super cells, which are composed of two or more slightly different or asymmetrical individual unit cell structures [11–14]. Multi-band metamaterials are obtained by these approaches in the expense of either increased electrical size or increased structural complexity. In metamaterial design, having small electrical size is important not only for miniaturisation concern but also to satisfy the conditions for the effective medium approach. Simplicity of the unit cell geometry is another design requirement needed for lower fabrication errors especially at shorter wavelengths of terahertz regime.

This paper introduces an electrically small and geometrically simple multi-resonant MNG metamaterial topology called *M*-band-nested *U*-ring resonator (*M*-NURR). As the name implies, the *M*-NURR unit cell is composed of *M*-nested *U*-rings printed on a dielectric substrate to obtain *M* distinct but closely located resonance frequencies. In general, a time-varying incident magnetic field having a component normal to the surface of a split-ring (1-NURR cell of this paper or the single-ring SRR cell) induces a magnetic dipole with a circulating current along the conducting ring. At the same time, charge densities with opposite polarities are induced across the split ends of the ring. Owing to the resulting inductive and capacitive effects, the metamaterial cell behaves as a series *LC* resonant circuit with resonance frequency $\omega_0 = 2\pi f_0 = (LC)^{-1/2}$. As discussed in [15, 16], at frequencies well below the resonance, response of the induced magnetic dipole is in phase with the incident field showing paramagnetic

© The Institution of Engineering and Technology 2012

response. As the frequency of external field approaches the resonance frequency, magnetic dipole moment begins to lag. At a certain value above the resonance frequency, the induced dipole moment becomes completely out of phase with the excitation field resulting in a diamagnetic response with permeability values smaller than unity or even smaller than zero. This phenomenon is explained by the Lorentz oscillator model and, the real part of the complex-valued effective permeability function is said to have the Lorentzian form displaying negative permeability values over a narrow frequency band. Similarly, each nested *U*-ring of the *M*-NURR cell leads to an individual resonance giving rise to a separate negative permeability region. Unless those resonance frequencies are too close to each other (sufficiently close to have overlapping resonance curves, for instance), each resonance frequency of the *M*-NURR topology is strongly associated with a specific *U*-ring and it can be efficiently tuned by changing the arm length of this *U*-ring only with negligible effects on the rest of the resonance frequencies. In conventional SRR-based multi-band metamaterial structures, changing any design parameter affects all of the resonance frequencies to some notable extent because of both geometry and the inter-cell coupling effects. To the best of our knowledge, having 'almost independently controllable resonance frequencies' is an important advantage of the proposed *M*-NURR structure not demonstrated in the other multi-band metamaterial designs reported in the literature.

2 Design, simulations and measurements

As the first step of design, fabrication and characterisation process, basic topology and design parameters of the *M*-NURR unit cell are defined as shown in Fig. 1*a* for $M = 3$ case, which are the side length of square-shaped

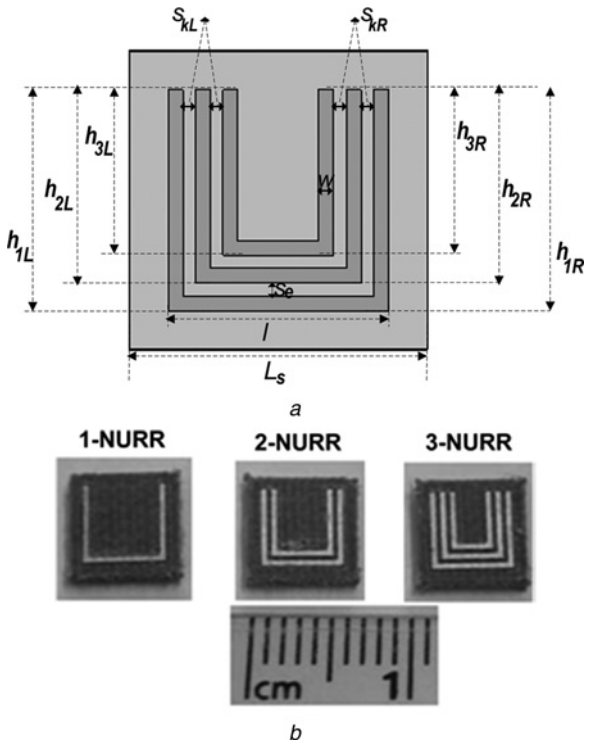


Fig. 1 *Designed and fabricated M-NURR unit cells*

a Design parameters shown for a 3-NURR unit cell
b Photographs of the fabricated *M*-NURR unit cells for $M = 1$, 2 and 3

substrate (L_s), base length of the outer *U*-ring (l), arm lengths of the *U*-rings (h_{1L}, h_{2L}, h_{3L}) on the left side and (h_{1R}, h_{2R}, h_{3R}) on the right side of the cell, width of the metal strips (w), vertical separation distance between the rings (s_e), horizontal separation distances between the rings (s_{kL}) on the left-side and (s_{kR}) on the right-side of the 3-NURR cell. Additional design parameters are conductivity (σ) and thickness (t) of the metal traces as well as relative permittivity (ε_r), thickness (d) and loss tangent ($\tan\delta$) of the substrate. In this study, we have used Arlon AD-300A type substrate with copper metallisation having parameters $\varepsilon_r = 3$, $d = 1.016$ mm, $\tan\ \delta = 0.002$, $\sigma = 5.8 \times 10^7$ S/m, $t = 0.035$ mm to design and fabricate three unit cells, 1-NURR, 2-NURR and 3-NURR (for the cases $M = 1$, 2, 3) with parameter values $L_s = 6.5$ mm, $w = 0.32$ mm, $s_e = s_{kL} = s_{kR} = 0.28$ mm, $l = h_{1L} = h_{1R} = 4.8$ mm, $h_{2L} = h_{2R} = 4.2$ mm and $h_{3L} = h_{3R} = 3.6$ mm by using LPKF-ProtoMat-H100 circuit board plotter. Photographs of the fabricated unit cells are shown in Fig. 1*b*.

In this work, we have used CST Microwave Studio, which is a commercial full-wave electromagnetic solver, for numerical simulation of the designed *M*-NURR arrays within an *X*-band rectangular waveguide setup that is used for experimental characterisation of the fabricated *M*-NURR prototypes. The complex valued *S*-parameters of these metamaterial structures are first computed by CST Microwave Studio and then measured by a network analyser (Agilent 8750D) that is combined with the waveguide setup. The *M*-NURR unit cell is placed at the centre of the measurement waveguide as shown in Fig. 2*a* so that its *LC* resonances are magnetically excited by the H_x magnetic field component of the fundamental TE_{10} waveguide mode (as anticipated by the Faraday's law) over the single mode operation range extending from 6.56 to 13.73 GHz. An infinitely large double-periodic *M*-NURR array is simulated by this measurement setup based on the well-known imaging effect of the copper walls of the waveguide. This real-world scenario is modelled in CST simulations by imposing perfect electric conductor (PEC) type boundary conditions at all four boundaries of the computational volume as shown in Fig. 2*a*. Dimensions of this *X*-band waveguide determine the spatial periods, $p_E = 10.16$ and $p_H = 22.86$ mm, of the simulated *M*-NURR array along the *y*- and *x*-axes, respectively. Photograph of the waveguide set up is shown in Fig. 2*b* indicating sample holder part's length as $p_k = 12.8$ mm along the propagation direction.

Simulated and measured transmission spectra ($|S_{21}|$ against frequency) as well as reflection spectra ($|S_{11}|$ against frequency) for the 1-NURR array are presented in Fig. 3*a* displaying only one resonance at 8.59 GHz in simulations and at 8.62 GHz in measurements with only 0.35 per cent error. Next, similar results for the 2-NURR are presented in Fig. 3*b* verifying the presence of two closely located resonances at 8.26 and 10.05 GHz in simulations, and at 8.59 and 10.33 GHz in measurements. Finally, the simulated and measured transmission and reflection spectra of 3-NURR are given in Fig. 3*c* with three distinct resonances at 8.24, 9.86 and 12.42 GHz in simulations and at 8.58, 10.31 and 12.79 GHz in experiments, respectively. In case of 2-NURR and 3-NURR characterisations, errors between simulated and measured resonance frequencies are found within acceptable limits (<5%in the worst case) but they are not as small as the error observed in the case of 1-NURR characterisations. These relatively higher errors can be explained by the presence of small ring-to-ring

© The Institution of Engineering and Technology 2012

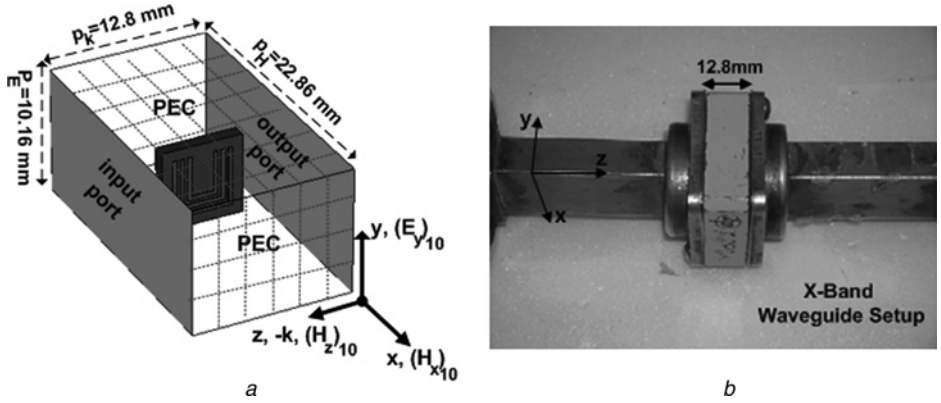


Fig. 2 *X-band waveguide setup used for numerical and experimental characterisations*

a Simulation setup
b Measurement setup

separations (s_{kL}, s_{kR} and s_e) in the 2-NURR and 3-NURR topologies. It is quite possible that small deviations may occur in the values of design parameters because of fabrication errors. As to be demonstrated in Section 3.1, small variations in these separation distances may cause notable shifts in resonance frequencies of the 3-NURR structure. Numerical errors because of mesh generation schemes may also occur in simulations contributing to differences between measured and computed resonance frequencies especially when a simulated *M*-NURR structure contains very fine details such as those narrow gaps between the nested *U*-rings.

Simulated and measured absorbance spectra $A(f) = 1 - |S_{11}(f)|^2 - |S_{21}(f)|^2$ of the 3-NURR array are also presented in Fig. 3*d* to illustrate the extent of overall losses caused by non-zero conductivity of the dielectric substrate material and the finite conductivity of thin layers of copper inclusions. Metamaterials are known to be lossy structures, in general. Although their loss characteristics may limit the use of metamaterials in some applications, this drawback can be turned into an advantage in the design of metamaterial absorbers [17].

As demonstrated in Figs. 3*a*–*c*, transmission spectrum of an *M*-NURR structure contains *M* distinct and narrow stop bands which make this topology a natural candidate for the design of multiple-stop-band filters and possibly multi-band notch filters. As a matter of fact, with its simple geometry, small electrical size and easily tuned multi-band capabilities, the *M*-NURR topology should be expected to be useful in all microwave and terahertz applications such as metamaterial absorbers [17], band-pass filters [18], band-stop filters [19] and antennas [20, 21] which are already demonstrated for the ordinary SRR and complementary SRR topologies.

Additional simulation results are presented in Figs. 4 and 5 to investigate the nature of resonances of the 3-NURR array.

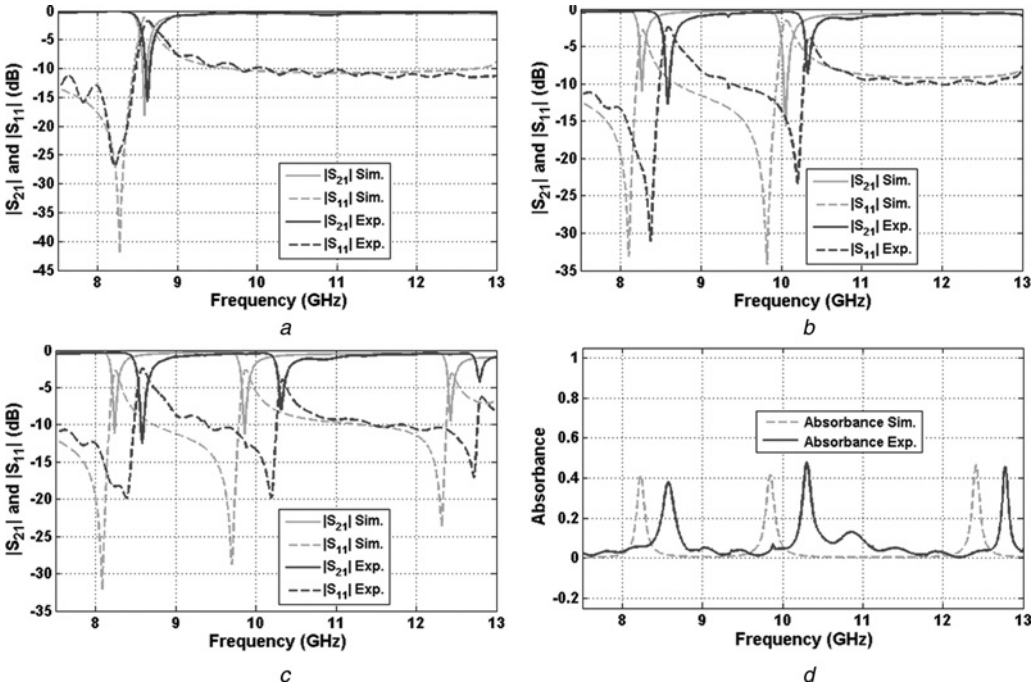


Fig. 3 *Simulated and measured spectra of transmission, reflection and absorbance*

a Transmission and reflection for the 1-NURR array
b Transmission and reflection for the 2-NURR array
c Transmission and reflection for the 3-NURR array
d Absorbance for the 3-NURR array

© The Institution of Engineering and Technology 2012

doi: 10.1049/iet-map.2012.0037

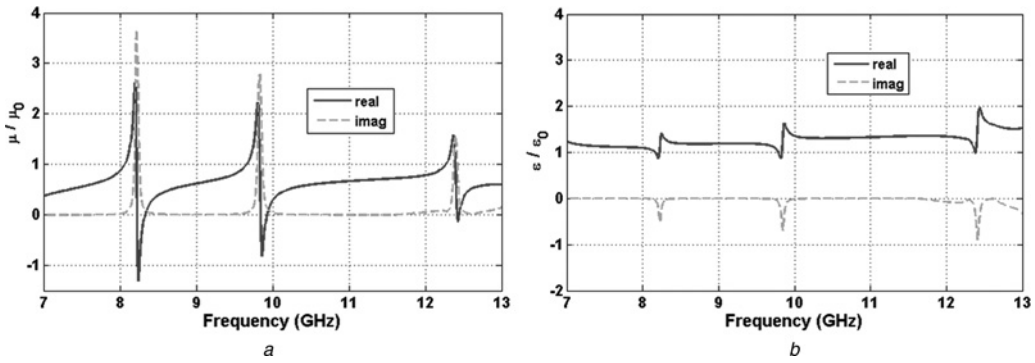


Fig. 4 *Complex effective medium parameters*

a Relative permeability
b Relative permittivity

Real and imaginary parts of the complex valued retrieved relative permeability $\mu/\mu_0 = \mu' + j\mu''$ and relative permittivity $\varepsilon/\varepsilon_0 = \varepsilon' + j\varepsilon''$ are plotted as a function of frequency in Figs. 4*a* and *b*, respectively. Parameter retrieval approach described in [22] is used to obtain these results for $\exp(-j\omega t)$ time-dependence. Real part of relative permeability μ' is obtained to be negative over three distinct resonance bands around frequencies 8.24, 9.86 and 12.42 GHz as seen in Fig. 4*a* indicating the magnetic nature of the associated resonances. In the meantime, imaginary part of permeability μ'' is obtained to be positive (i.e. $\mu'' > 0$) over these resonance bands as expected for a passive medium. The slight, negligible anti-resonance features observed in Fig. 4*b* in the effective permittivity curves in resonance regions may be explained by the general theory of effective media [23] as an artefact resulting from the periodical nature of this sparse 3-NURR array (see Fig. 2*a* for the values of spatial periods). Regarding the bandwidths of resonance curves and the associated negative-permeability (MNG) regions, the 3-NURR design of this paper (see Figs. 3*c* and 4) and the super-cell type SRR-based design reported in [13] (see Fig. 14(a) and Fig. 15 in that reference) have quite similar performances. MNG bands of both multi-band metamaterial structures are found narrow having bandwidths ~100 MHz. This comparison is particularly meaningful as the same *X*-band rectangular waveguide setup is used in the characterisation of both metamaterial topologies leading to the same sparse array design. Use of denser metamaterial arrays is expected to be helpful to increase the metamaterial bandwidth for both SRR-based and *M*-NURR type-structures. It should also be emphasised that the highly compact and geometrically simpler design of the 3-NURR structure is superior to the SRR-based triple-band metamaterial of [13] for the concerns of miniaturisation and ease of fabrication.

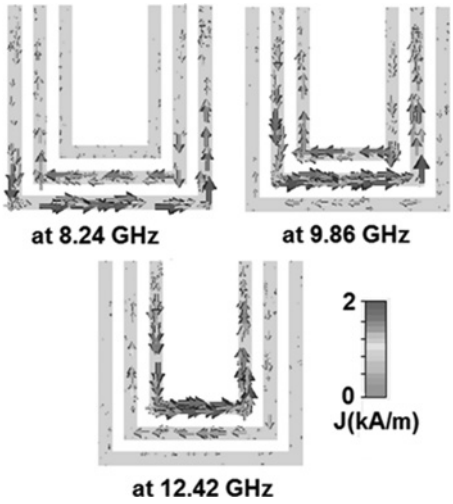


Fig. 5 *Surface current densities computed at each resonance frequency for the 3-NURR array*

As the final result of this section, Fig. 5 demonstrates the circulating behaviour of surface currents at each resonance frequency of the 3-NURR structure revealing the *LC* nature of these resonances. These current density plots also show that the resonance at $f_1 = 8.24$ GHz is strongly related to the current activity in the outermost *U*-ring while its value may be somewhat sensitive to the coupling effects caused by the presence of the middle ring. Similarly, the next resonance at $f_2 = 9.86$ GHz is primarily related to the currents flowing in the middle ring but also affected by the coupling effects introduced by the inner ring. The highest resonance at $f_3 = 12.42$ GHz is strongly associated with the innermost *U*-ring and it is very slightly affected by the coupling effects because of the middle ring.

3 Effects of design parameters on resonance frequencies

In this section, we will demonstrate the effects of the changing design parameters h_{1L}, h_{1R}, h_{2L}, h_{2R}, h_{3L}, h_{3R}, s_{kL}, s_{kR} and w on resonance frequencies f_1, f_2 and f_3 of the 3-NURR structure.

3.1 Effects of changing ring-to-ring separation distances on resonance frequencies

As the first parametric study, we will simulate the effects of inter-ring couplings on the values of resonance frequencies. Transmission spectra shown in Fig. 6 are obtained for different values of s_{kL} and s_{kR} (i.e. the horizontal separation distances between the *U*-rings) while keeping the size of the outer ring fixed. As the value for $s_{kL} = s_{kR}$ is increased from 0.24 to 0.32 mm symmetrically on both left and right sides of the 3-NURR cell, capacitive coupling between neighbouring rings decreases leading to lower equivalent capacitance values and hence higher resonance frequencies for the *LC* resonances, as expected. In fact, the shifts occurring in the lowest resonance frequency f_1 reflect the true inter-ring coupling effects in this parametric investigation scenario because only the outer ring does not experience any length change as $s_{kL} = s_{kR}$ varies. The base lengths of the middle and inner rings decrease as $s_{kL} = s_{kR}$ increases

© The Institution of Engineering and Technology 2012

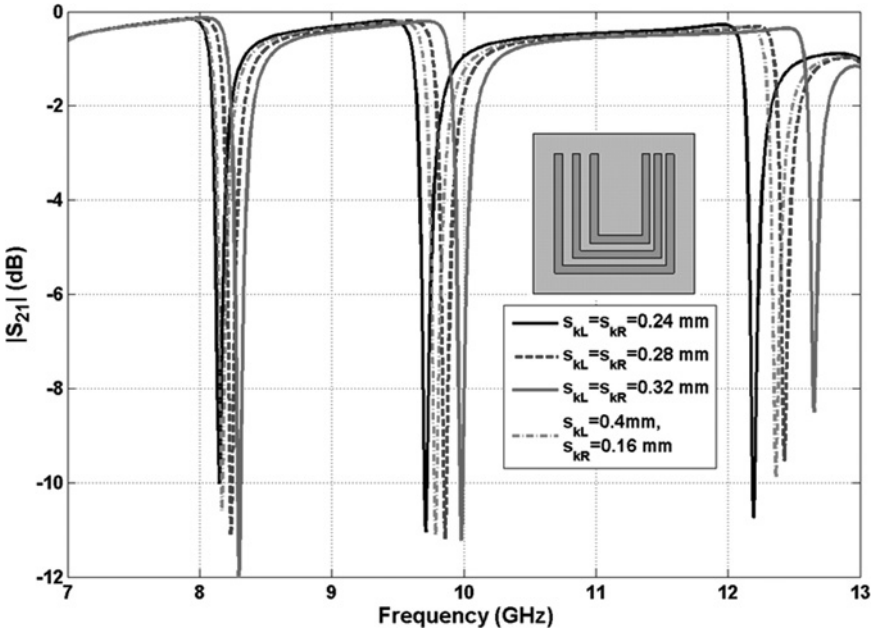


Fig. 6 *Transmission spectra of the symmetrical and asymmetrical 3-NURR topologies for different values of the ring-to-ring spacing parameter (the asymmetrical cell is shown in the inset)*

leading to smaller effective inductance values and hence, more pronounced increases in f_2 and especially in f_3 as observed in Fig. 6. This parametric study is also helpful to explain the differences between the numerical and experimental values of resonance frequencies observed in Figs. 3*b* and *c* for 2-NURR and 3-NURR arrays, respectively.

Next, the ring-to-ring distance parameters are assigned asymmetrically to be $s_{kL} = 0.4$ mm between the ring arms on the left-side and $s_{kR} = 0.16$ mm on the right-side of the asymmetrical 3-*NURR* cell, which is shown as the inset in Fig. 6. When we specifically choose to have $s_{kL} + s_{kR} = 2s_k = 0.56$ mm instead of having $s_{kL} = s_{kR} = s_k = 0.28$ mm, the middle and inner *U*-rings are simply pushed to the right without changing the overall lengths of individual *U*-rings. Therefore any shifts observed in resonance frequencies would be entirely because of the induced left/right asymmetry of ring-to-ring distances. As seen in Fig. 6, the simulated transmission spectra for these comparable symmetrical and asymmetrical 3-NURR topologies are very close to each other with negligible shifts ($<0.7\%$) in resonance frequencies.

3.2 Effects of changing the metal line width on resonance frequencies

Secondly, we have investigated the effects of changing metal strip width w on the resonance frequencies. The transmission spectra shown in Fig. 7 are obtained for different values of w while keeping the outer boundary of the largest ring fixed. When w is increased from 0.24 to 0.32 mm, self-inductances of the *U*-rings decrease resulting in higher resonance frequencies as shown in the figure. More

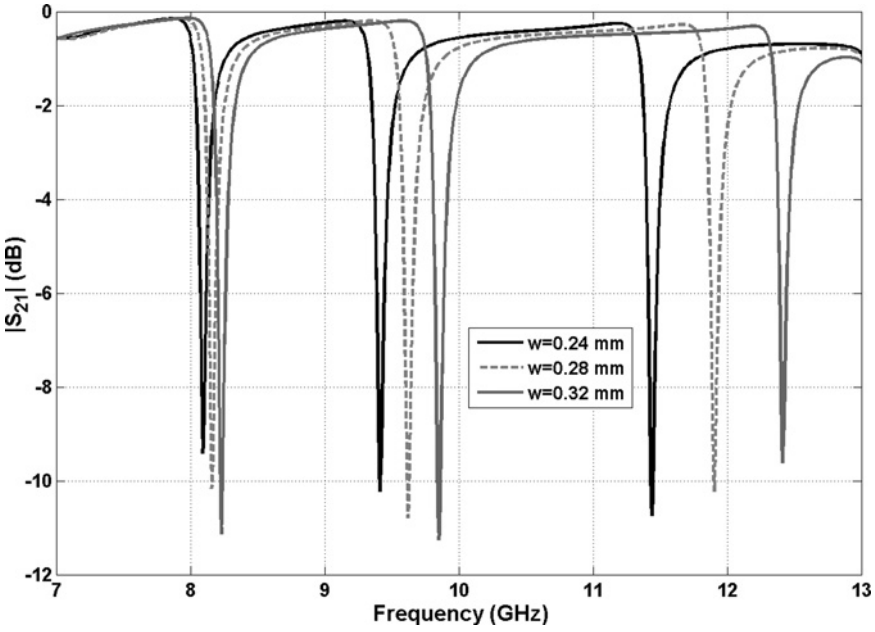


Fig. 7 *Transmission spectra of the 3-NURR for different values of metal line width*

© The Institution of Engineering and Technology 2012

doi: 10.1049/iet-map.2012.0037

pronounced increases in f_2 and especially in f_3 are observed in Fig. 7 because the lengths of the middle and inner rings are somewhat decreased while w is increased in this demonstration. This, in turn, makes equivalent inductances decrease more and hence resonance frequencies f_2 and f_3 increase more evidently.

3.3 Effects of changing the arm lengths on resonance frequencies

In Sections 3.1 and 3.2, we have shown that changing either metal strip width or separation between the neighbouring metal strips causes variations in all resonance frequencies of a symmetrically designed 3-band *U*-ring resonator. Actually, this is a typical behaviour demonstrated in numerous metamaterial papers. In this section however, we will demonstrate that an arbitrarily selected resonance frequency of this 3-NURR structure can be shifted to higher or lower frequencies by changing the arm length of the associated *U*-ring with negligible effects on the rest of the resonances. Owing to this important property, resonances of an *M*-NURR metamaterial can be adjusted almost independently and in a highly controlled manner. For the proof of concept, transmission spectra of 3-NURR are simulated for three different $h_{1L} = h_{1R}$ (arm lengths of the outer *U*-ring) values and the results are plotted in Fig. 8*a*. It is clearly seen that increasing $h_{1L} = h_{1R}$ from 4.8 to 5.0 mm (or to 5.2 mm) on both sides symmetrically makes the lowest resonance frequency f_1 decrease whereas the other two resonance frequencies are affected negligibly. Similarly, increasing $h_{2L} = h_{2R}$ (arm lengths of the middle *U*-ring) affects only the second resonance frequency f_2 as seen in Fig. 8*b*. Finally, increases in $h_{3L} = h_{3R}$ (arm lengths of the inner *U*-ring) cause reductions in the highest resonance frequency f_3 only, without affecting the other resonances, as shown in Fig. 8*c*. These results are important as they clearly show that value of each resonance frequency can be adjusted almost independently and in a highly controlled manner by changing the arm length of the associated *U*-ring. This behaviour of the *M*-NURR topology would be impaired if the resonance frequencies are too close to each other with almost overlapping resonance curves.

Effect of asymmetry in the left/right-arm lengths of the 3-NURR cell is additionally investigated in this section as follows: The asymmetrical 3-NURR cell having unequal outer arm lengths $h_{1L} = 4.8$ mm and $h_{1R} = 5.2$ mm has the same overall outer ring length as the symmetrical 3-NURR cell that has $h_{1L} = h_{1R} = 5.0$ mm. These two length-wise equivalent topologies have almost identical transmission spectra as shown in Fig. 8*a*. Similar results are presented in the same figure for the asymmetrical cell with $h_{1L} = 4.8$ mm and $h_{1R} = 5.6$ mm and its symmetrical equivalent with $h_{1L} = h_{1R} = 5.2$ mm. Additional simulation results for asymmetrical 3-NURR cells with unequal left/right-arm lengths in the middle and in the inner *U*-rings are demonstrated in Figs. 8*b* and *c*, respectively. Based on all these simulation results, it is concluded that resonance frequencies of the 3-NURR structure are negligibly affected by the left/right asymmetry as long as the individual ring lengths are kept the same.

Finally, by adjusting arm lengths of the individual *U*-rings, three distinct resonances of the 3-NURR structure are merged into one for the purpose of enhancing the MNG bandwidth. In this application, arm lengths of the outer, middle and inner rings of the 3-NURR cell are chosen to be $h_{1L} = h_{1R} = 4.5$ mm, $h_{2L} = h_{2R} = 4.02$ mm and $h_{3L} = h_{3R} = 3.54$ mm, respectively, to realise three distinct resonances at 8.56, 9.96 and 11.97 GHz as seen in Fig. 9*a*. Then, while keeping the value $h_{2L} = h_{2R} = 4.02$ mm fixed, the arm length of the outer ring is decreased to $h_{1L} = h_{1R} = 3.58$ mm and the arm length of the inner ring is increased to $h_{3L} = h_{3R} = 4.64$ mm to merge all three resonances around 10 GHz as shown in Fig. 9*a*. In this parametric design process, the ring-to-ring separation parameters are chosen to be $s_e = s_{kL} = s_{kR} = 0.16$ mm to

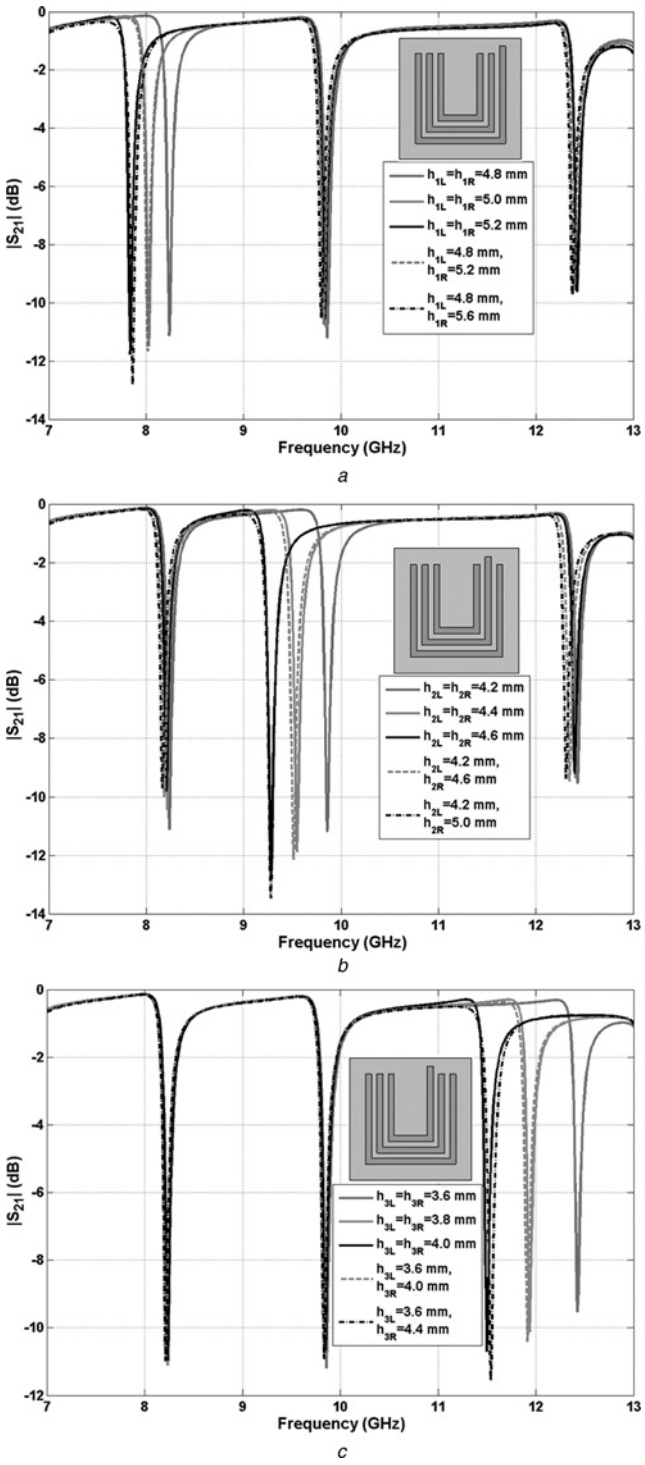


Fig. 8 *Transmission spectra of the symmetrical and asymmetrical 3-NURR topologies for different arm lengths (views of asymmetrical U-ring cells are shown as insets)*

a Varying h_{1L} and h_{1R} only
b Varying h_{2L} and h_{2R} only
c Varying h_{3L} and h_{3R} only

© The Institution of Engineering and Technology 2012

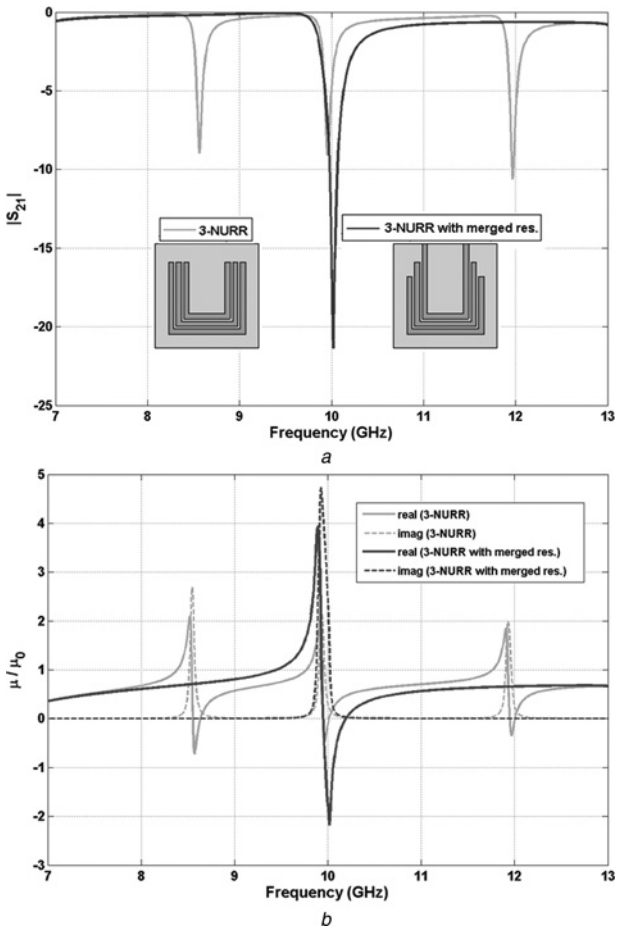


Fig. 9 *Transmission spectra and relative permeability curves for two different 3-NURR designs with distinct and merged frequencies*

a Transmission spectra
b Relative permeability curves

keep the elongated inner ring arms within the unit cell boundaries without changing the substrate dimensions. The transmission spectra for the original and tuned 3-NURR structures are plotted in Fig. 9*a* while the corresponding retrieved relative permeability curves are shown in Fig. 9*b*. As seen in these results, the merged resonance at 10 GHz is much stronger than each of the original distinct resonances, leading to an almost three times wider MNG bandwidth with much deeper negative permeability values extending up to a level of −2.

4 Conclusion

In this study, we have demonstrated a novel multi-band metamaterial topology, called *M*-NURR, composed of *M* concentric *U*-rings. For the proof of concept, three different symmetrical *M*-NURR structures (for $M = 1, 2, 3$) are simulated, fabricated and experimentally verified to obtain *M*-distinct *LC*-type magnetic resonances in X-band. In addition to having an electrically small and geometrically simple unit cell topology, this *M*-NURR resonator structure is proven to have the flexibility to control each of *M* closely located resonance frequencies almost independently by simply changing the arm length of the associated *U*-ring. Even in asymmetrical NURR topologies, lengths of individual *U*-rings are shown to be imperative in determining the resonance frequencies. It is demonstrated as an application of this easy-tuning capability that distinct resonances of the 3-NURR structure can be merged to obtain a single and much stronger resonance accompanied by an almost three times wider MNG bandwidth. This special tuning property of the proposed sub-wavelength *M*-NURR metamaterial topology is expected to be very useful to tailor the frequencies of operation with high resolution in the design of miniaturised multi-band mobile communication devices in future studies.

5 References

1 Pendry, J.B., Holden, A.J., Robbins, D.J., Stewart, W.J.: 'Low frequency plasmons in thin-wire structures', *J. Phys. Condens. Matter*, 1998, **10**, (22), pp. 4785–4809
2 Marqués, R., Mesa, F., Martel, J., Medina, F.: 'Comparative analysis of edge- and broadside-coupled split ring resonators for metamaterial design-theory and experiments', *IEEE Trans. Antennas Propag.*, 2003, **51**, (10), pp. 2572–2581
3 Shelby, R.A., Smith, D.R., Schultz, S.: 'Experimental verification of a negative index of refraction', *Science*, 2001, **292**, pp. 77–79
4 Bilotti, F., Toscano, A., Vegni, L.: 'Design of spiral and multiple split-ring resonators for the realization of miniaturized metamaterial samples', *IEEE Trans. Antennas Propag.*, 2007, **55**, (8), pp. 2258–2267
5 Yuan, Y., Bingham, C., Tyler, T., *et al.*: 'A dual-resonant terahertz metamaterial based on single-particle electric-field-coupled resonators', *Appl. Phys. Lett.*, 2008, **93**, p. 191110(1)–191110(3)
6 Chowdhury, D.R., Singh, R., Reiten, M., *et al.*: 'A broadband planar terahertz metamaterial with nested structure', *Opt. Express*, 2011, **19**, (17), pp. 15817–15823
7 Geschke, R.H., Jokanovic, B., Meyer, P.: 'Compact triple-band resonators using multiple split-ring resonators'. Proc. 39th European Microwave Conf., Rome, Italy, 2009, pp. 366–369
8 Ekmekci, E., Turhan-Sayan, G.: 'Single loop resonator: Dual-band magnetic metamaterial structure', *Electron. Lett.*, 2010, **46**, (5), pp. 324–325
9 Yurduseven, O., Yilmaz, A.E., Turhan-Sayan, G.: 'Triangular-shaped single-loop resonator: A triple-band metamaterial with MNG and ENG regions in S/C bands', *IEEE Antennas Wirel. Propag. Lett.*, 2011, **10**, pp. 701–704
10 Yurduseven, O., Yilmaz, A.E., Turhan-Sayan, G.: 'Hybrid-shaped single-loop resonator: a four-band metamaterial structure', *Electron. Lett.*, 2011, **47**, (25), pp. 1381–1382
11 Chen, H., Ran, L., Huangfu, J., *et al.*: 'Metamaterial exhibiting left-handed properties over multiple frequency bands', *J. Appl. Phys.*, 2004, **96**, (9), pp. 5338–5340
12 Wang, J., Qu, S., Yang, Y., Ma, H., Wu, X., Xu, Z.: 'Multiband left-handed metamaterials', *Appl. Phys. Lett.*, 2009, **95**, pp. 014105(1)–014105(3)
13 Ekmekci, E., Topalli, K., Akin, T., Turhan-Sayan, G.: 'A tunable multi-band metamaterial design using micro-split SRR structures', *Opt. Express*, 2009, **17**, (18), pp. 16046–16058
14 Zhu, C., Ma, J.J., Li, L., Liang, C.H.: 'Multiresonant metamaterial based on asymmetric triangular electromagnetic resonators', *IEEE Antennas Wirel. Propag. Lett.*, 2010, **9**, pp. 99–102
15 Smith, D.R., Padilla, W.J., Vier, D.C., Nemat-Nasser, S.C., Schultz, S.: 'Composite medium with simultaneously negative permeability and permittivity', *Phys. Rev. Lett.*, 2000, **84**, (18), pp. 4184–4187
16 Yen, T.J., Padilla, W.J., Fang, N., *et al.*: 'Terahertz magnetic response from artificial materials', *Science*, 2004, **303**, pp. 1494–1496
17 Landy, N.I., Sajuyigbe, S., Mock, J.J., Smith, D.R., Padilla, W.J.: 'Perfect metamaterial absorber', *Phys. Rev. Lett.*, 2008, **100**, pp. 207402(1)–207402(4)
18 Al-Naib, I.A.I., Jansen, C., Koch, M.: 'Miniaturized bandpass filter based on metamaterial resonators: a conceptual study', *J. Phys. D: Appl. Phys.*, 2008, **41**, pp. 205002(1)–205002(4)
19 García-García, J., Martin, F., Falcone, F., *et al.*: 'Microwave filters with improved stopband based on sub-wavelength resonators', *IEEE Trans. Microw. Theory Tech.*, 2005, **53**, (6), pp. 1997–2006
20 Kim, I.K., Varadan, I.K.: 'Electrically small, millimeter wave dual band meta-resonator antennas', *IEEE Trans. Antennas Propag.*, 2010, **58**, (11), pp. 3458–3463
21 Ghalibafan, J., Attari, A.R.: 'A new dual-band microstrip antenna with U-shaped slot', *Prog. Electromagn. Res. C*, 2010, **12**, pp. 215–223
22 Szabo, Z., Park, G.-H., Hedge, R., Li, E.-P.: 'A unique extraction of metamaterial parameters based on Kramers-Kronig relationships', *IEEE Trans. Microw. Theory Tech.*, 2010, **58**, (10), pp. 2646–2653
23 Liu, R., Cui, T.J., Huang, D., Zhao, B., Smith, D.R.: 'Description and explanation of electromagnetic behaviors in artificial metamaterials based on effective medium theory', *Phys. Rev. E*, 2007, **76**, pp. 026606(1)–026606(8)

© The Institution of Engineering and Technology 2012

doi: 10.1049/iet-map.2012.0037